GROWTH OF GROUPS OF WIND GENERATED WAVES

FREDERIQUE DRULLION

Department of Mathematics, Embry-Riddle Aeronautical University
Daytona Beach, FL 32114-3900, USA.

A high-Reynolds-number stress closure model is used to perform numerical simulations of the wind flow above different groups of waves. The group profiles can change as the individual waves grow within its envelop due to the energy transfer between the wind and the group. The focus of this study is the behavior of the critical layer and the associated "cat's-eye" structures centered around the critical height, where the real part of the complex wave speed is equal to the mean flow velocity. The position and size of these structures depend on the wave age and the wave steepness. It is shown that the larger the structures become, the more disturbance of the wind flow above the wave occurs. The results obtained here demonstrate the formation of cat's-eye structures which appear asymmetrically over the waves within a group.

AMS (MOS) Subject Classification. 39A10.

1. Introduction

The question of growth and decay of wind generated waves in the ocean has been studied extensively but the interactions and energy transfer between the water wave and the ambient wind is still not fully understood. Most of the studies (experimental, numerical or analytical) consider monochromatic or idealized wave profiles. As it has been observed extensively, waves actually travel in groups for which the profiles change as the waves in their envelop are traveling. In this study we are considering the influence of grouping on the growth of ocean waves induced by wind shear flows. We focus our attention to the region around the height were the real part of the complex wave speed is equal to the mean flow velocity. This region, called the "critical layer", is the central point in Miles' theory [1] and Lighthill's interpretation of growth of waves [2]. Miles stated that the amount of energy transferred from the surrounding wind to the waves is proportional to the value of the curvature of the velocity profile at the critical height. In this region closed streamlines structures called "cat's-eyes" are developed. The larger these structures are, the more disturbance of the wind flow above the wave occurs. In some previous work [3], a high-Reynolds-number stress closure model over a moving idealized wavy surface was used to show that their size and position are dependent on the wave age and wave steepness, which is

in accordance with direct numerical simulations results [4]. In this study, we use the same Reynolds stress model over different groups of waves to determine the height of the critical layer and the overall shape, size and position of the cat's-eye structures which develop over individual waves within the group envelop.

2. Governing equations

The air flow with density ρ_a and kinematic viscosity ν_a over the group of waves is governed by the incompressible Reynolds averaged Navier-Stokes equations:

$$(2.1) \qquad\qquad \frac{\partial U_i}{\partial x_i} = 0$$

$$(2.2) \qquad \frac{DU_i}{Dt} = -\frac{1}{\rho_a}\frac{\partial P}{\partial x_i} + \frac{\partial}{\partial x_j}\left[\nu_a\left(\frac{\partial U_i}{\partial x_j} + \frac{\partial U_j}{\partial x_i}\right) - \overline{u_i'u_j'}\right]$$

where U_i is the mean velocity component in the x_i-direction, P is the mean pressure, $\overline{u_i'u_j'}$ is the Reynolds-averaged stress correlation and t is time.

A model for the Reynolds-averaged stress correlations is needed to close equation (2.2). A rational approach for providing a model for $\overline{u_i'u_j'}$ in equation (2.2) relies on its transport equation, which may be written in the following form

$$(2.3) \qquad\qquad \frac{D\overline{u_i'u_j'}}{Dt} = P_{ij} + \Pi_{ij} - \varepsilon_{ij} + d_{ij}$$

where $P_{ij} = -(\overline{u_i'u_k'}\partial U_j/\partial x_k + \overline{u_j'u_k'}\partial U_i/\partial x_k)$ is the production term, Π_{ij} represents the velocity-pressure gradient correlation, ε_{ij} the viscous dissipation, and d_{ij} represents diffusion by both molecular viscosity and the triple velocity moments. On the left-hand side of (2.3), the stress convection, and the production term are both exact and require no further modelling. However, all other terms contain further unknowns which must be modelled. For this we adopt a high-Reynolds-number turbulence model [5]. In this model, the pressure correlation Π_{ij} is decomposed into a redistributive part, ϕ_{ij}^*, and a non-redistributive part by

$$(2.4) \qquad \Pi_{ij} \equiv -\frac{1}{\rho_a}\left(\overline{u_i'\frac{\partial p'}{\partial x_j} + u_j'\frac{\partial p'}{\partial x_i}}\right) = \phi_{ij}^* + \frac{\overline{u_i'u_j'}}{2K}d_{kk}^p$$

where $d_{kk}^p = -(1/\rho_a)\partial\overline{u_k'p'}/\partial x_k$ represents the pressure diffusion of the turbulent kinetic energy $K = \frac{1}{2}\overline{u_i'u_i'}$.

The model employed for the redistributive part of the pressure correlation, ϕ_{ij}^*, is based on the cubic realizable form derived by Fu [6]. The dissipation ε_{ij} is modelled as

$$(2.5) \qquad\qquad \varepsilon_{ij} = \left(1 - A^{1/2}\right)\frac{\varepsilon}{K}\overline{u_i'u_j'} + \frac{2}{3}\varepsilon\delta_{ij}$$

where $A = 1 - 9/8(A_2 - A_3)$, $A_2 = a_{ij}a_{ij}$, $A_3 = a_{ij}a_{jk}a_{ki}$ and $a_{ij} = \overline{u_i'u_j'}/K - 2/3\delta_{ij}$. This is very similar to the form adopted in other high-Reynolds-number flows, see for example Gibson & Launder [7].

In (2.5) The dissipation rate ε is obtained from the solution of its own transport equation:

$$
\begin{aligned}
\frac{D\varepsilon}{Dt} &= c_{\varepsilon 1}\frac{\varepsilon P_{kk}}{2K} - c_{\varepsilon 2}\frac{\varepsilon^2}{K} + \frac{\partial}{\partial x_l}\left[\left(\nu_a\delta_{lk} + c_\varepsilon\overline{u_l'u_k'}\frac{K}{\varepsilon}\right)\frac{\partial\varepsilon}{\partial x_k}\right] \\
&\quad + c_{\varepsilon 3}A^{1/2}(1 - A)\frac{\varepsilon}{\sqrt{K}}\overline{u_i'u_j'}\frac{\partial A}{\partial x_i}\frac{\partial}{\partial x_j}\left(\frac{K^{3/2}A^{1/2}}{\varepsilon}\right)
\end{aligned}
$$

(2.6)

with coefficients

$$c_{\varepsilon 1} = 1.0, \quad c_{\varepsilon 2} = 1.92/(1 + 0.7A_dA_2^{1/2}), \quad A_d = \max(0.2, A), \quad c_{\varepsilon 3} = 1.0, \quad c_\varepsilon = 0.18$$

The only remaining term in the stress transport equations is the diffusion term

(2.7)
$$d_{ij} = \frac{\partial}{\partial x_k}\left(\nu_a\frac{\partial\overline{u_i'u_j'}}{\partial x_k} - \overline{u_i'u_j'u_k'}\right)$$

The viscous diffusion is, of course exact, and the triple correlations are modelled via the proposal of Hanjalic & Launder [8] proposal

(2.8)
$$\overline{u_i'u_j'u_k'} = -c_s\frac{K}{\varepsilon}\left[\overline{u_i'u_l'}\frac{\partial\overline{u_j'u_k'}}{\partial x_l} + \overline{u_j'u_l'}\frac{\partial\overline{u_i'u_k'}}{\partial x_l} + \overline{u_k'u_l'}\frac{\partial\overline{u_j'u_i'}}{\partial x_l}\right]$$

where $c_s = 0.11$.

3. Numerical scheme

The finite volume method is used to solve the governing equations. The volumes are non-orthogonal and collocated such that all flow variables are stored at the centered of the cells. The numerical scheme uses a pressure based solver [9]. A first order forward discretization in time is used, and the convective fluxes are approximated with the higher-order upstream-weighted scheme, QUICK of Leonard [10]. The pressure and diffusive fluxes are discretized using a central difference operator. The finite volume method and the chosen discretizations lead to penta-diagonal system solved using a tri-diagonal, matrix algorithm (TDMA).

The discretization is proceeded by a transformation of the Cartesian coordinates of the governing equations to the non-orthogonal coordinates ξ and ζ using the Jacobian transformation matrix. The transport equation for any scalar property Φ many
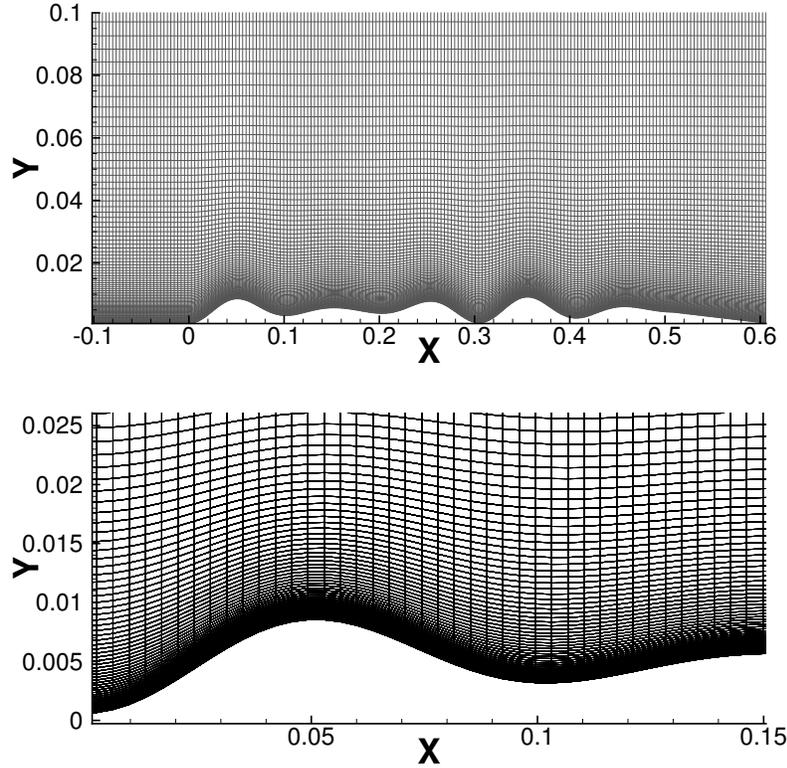
FIGURE 1. Computational mesh

be expressed in non-orthogonal direction as

$$(3.1) \quad \underbrace{\frac{\partial}{\partial t}(J\rho_a\Phi)}_{\text{transient term}} + \underbrace{\frac{\partial}{\partial \xi}\left(\rho_a U^{(\xi,\zeta)}\Phi\right) + \frac{\partial}{\partial \zeta}\left(\rho_a W^{(\xi,\zeta)}\Phi\right)}_{\text{convection}}$$

$$+ \underbrace{\frac{\partial}{\partial \xi}\left(\alpha_\Phi J \frac{\partial \Phi}{\partial \xi}\right) + \frac{\partial}{\partial \zeta}\left(\beta_\Phi J \frac{\partial \Phi}{\partial \zeta}\right)}_{\text{diffusion}} = \underbrace{J S_\Phi}_{\text{source}}$$

where $U^{(\xi,\zeta)} = Uz_\zeta - Wx_\zeta$ and $W^{(\xi,\zeta)} = Wx_\xi - Uz_\xi$ are contravarient velocity components, J is the Jacobian of the transformation, S_Φ is the source term including diffusive terms, pressure terms in the momentum equation, $\alpha_\Phi = \Gamma_\Phi(x_\zeta^2 + z_\zeta^2)$, $\beta_\Phi = \Gamma_\Phi(x_\xi^2 + z_\xi^2)$, where Γ_Φ is isotropic diffusivity, and the subscripts ξ, ζ denote partial differentiations.

The mesh covering the computational domain contains 200×100 nodes and extends over six wavelengths in horizontal direction and two wavelength in the vertical direction. As can be seen from figure 1, it is refined near the water surface in order to capture the steep gradients which are inherently present there.

4. **Problem set up and group construction**

We consider groups of waves composed by superposition of three cosine waves (see equation 4.2 below). The groups are traveling in deep water at the speed $c_r = \dfrac{1}{2}\sqrt{\dfrac{g}{k}}$ and a wind whose mean velocity is assumed to be logarithmic is blowing above them. At the height of one wavelength above the surface of the wave, the wind velocity is imposed to be U_λ.

The turbulent flow has a mean velocity profile $U(\zeta) = U_1 \ln(\zeta/\zeta_0)$, $U_1 \equiv U_*/\kappa$, U_* being the friction velocity, κ being the von Kármán's constant, and ζ_0 is the surface roughness. Note that, ξ and ζ are the wave-following coordinates, given by the following transformation

$$(4.1) \qquad\qquad x = \xi, \qquad z = \zeta + h(\xi, \zeta)$$

where $h = h(\xi, \zeta)$ maps $z = h_0$ onto $\zeta = 0$ and is evanescent for $k\zeta \uparrow \infty$ but is otherwise arbitrary. The computational domain is taken to six wavelengths horizontally and two wavelengths vertically. The groups only extend over four wavelengths (from $x = 0$ to $x = 4\lambda$) and are surrounded by a flat surface. The latter ensures the periodicity in boundary conditions in the x-direction. In our simulations, the frame of reference is traveling with the group. The initial wave group profile is given by:

$$(4.2) \qquad\qquad h_0 = a[\cos(k\mathcal{X}) + \epsilon_1 \cos(k_1 \mathcal{X}) + \epsilon_2 \cos(k_2 \mathcal{X})]$$

where a is the initial wave amplitude k is the wave number, $k_1 = 1 + \sqrt{2}ak$ and $k_2 = 1 - \sqrt{2}ak$ and where $\mathcal{X} = \xi - c_r t$.

5. **Boundary conditions**

A strictly horizontal velocity $U = U_\lambda - \dfrac{c_r}{2}$ is imposed at the top of the computational domain, taking into account the fact that the frame of reference is moving with the waves at the speed $\dfrac{c_r}{2}$.

At the bottom of the domain, the mean velocity components match the wave orbital velocities. The orbital velocities for $0 \le x \le 4\lambda$, are given by

$$
\begin{aligned}
u &= -c_g ak[\cos(kx) + \epsilon_1 k_1 \cos(k_1 x) + \epsilon_2 k_2 \cos(k_2 x)] - c_g \\
v &= -c_g ak[\sin(kx) + \epsilon_1 k_1 \sin(k_1 x) + \epsilon_2 k_2 \sin(k_2 x)]
\end{aligned}
$$

Note that, for the flat surfaces surrounding the group portion on the south boundary, namely when $x < 0$ and $x > 4\lambda$, we impose the conditions $u = -c_g$ and $v = 0$. In the streamwise direction, periodic boundary conditions are imposed on all the mean variables and the turbulent stresses together with the turbulent dissipation rate. At the top and the bottom of the computational domain the boundary conditions imposed on the stresses and the dissipation rate are the same as the one used in [11].
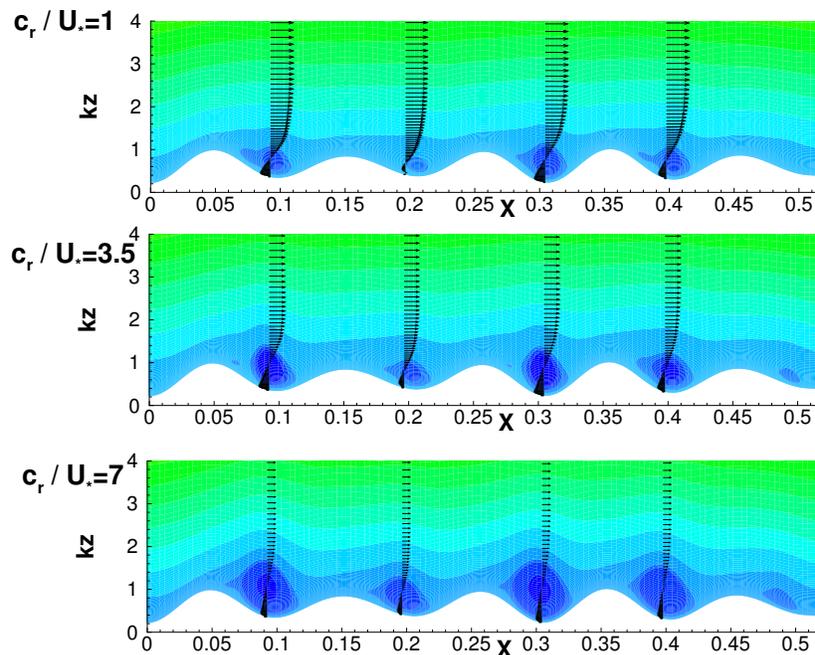
FIGURE 2. Contour plots and velocity vector field of the stream function over *group1* wave for three values of the wave age c_r/U_*=1 (top); 3.5 (middle), and 7 (bottom).

The boundary conditions for stresses and dissipation rate is taken from our earlier paper [11].

6. Results

In this paper we report computations of turbulent flow over two groups, in a frame of reference moving with the wave, namely *group1* and *group2*. For both groups, the initial amplitude of the main cosine wave is $a(0) = 0.0025m$ and its wavelength is $\lambda = 0.1016m$. $(\epsilon_i)_{1,2}$ for *group1* and *group2* are respectively: ($\epsilon_1 = 0.2$, $\epsilon_2 = 0.1$) and ($\epsilon_1 = 0.25$, $\epsilon_2 = 0.5$).
Note that, for all the diagrams, the vertical axis has been normalized using the fundamental wave number k.

6.1. **Non growing groups.** We first consider the influence of the wave age on the cat's-eye structures over non-growing groups for the following three wave ages: $c_r/U_* = 1$, $c_r/U_* = 3.5$, and $c_r/U_* = 7$.

Figures 2 and 3 show the contour plots of the stream function for respectively *group1* and *group2* as a function for three wave ages $c_r/U_* = 1, 3.5$ and 7. As it can be seen from these figures, at lowest value of c_r/U_* cat's-eye structures are formed downstream of the steepest waves in the group. As the wave age increases to 3.5, we note that new weaker cat's-eye structures appear in the lee of the waves where
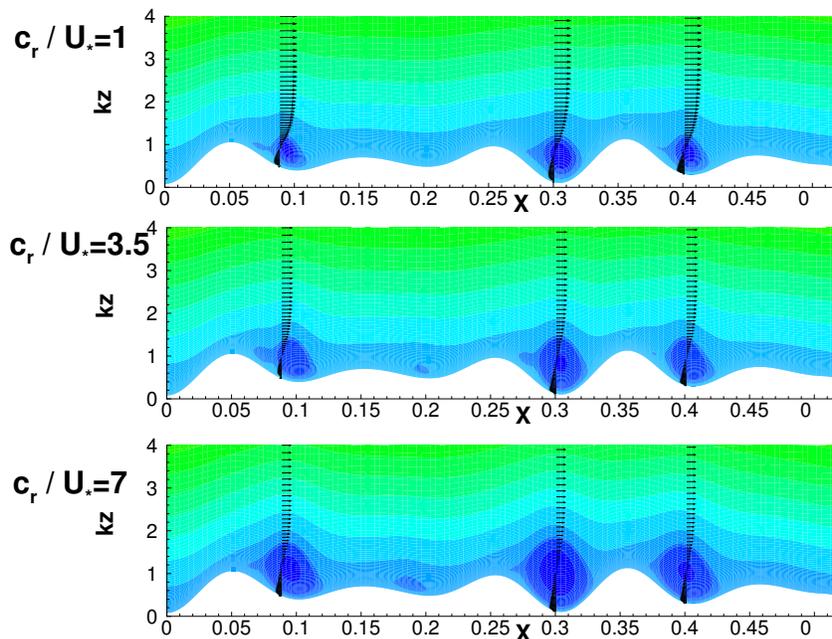
FIGURE 3. Contour plots of stream function and velocity vector field over *group2* wave for three values of the wave age $c_r/U_* = 1$ (top); 3.5 (middle), and 7 (bottom).

they were not previously present, the pre-existing structures increase in size and their center slightly shift toward the peak of the wave behind of them, the cat's-eye structures also slightly lift up from the surface of the wave. At $c_r/U_* = 7$ the cat's-eye become stronger and move further over the peak of the waves in the group. At the largest value of the wave age we can observe a maximum disturbance of the mean flow above the waves, the critical height, passing through the center of the cat's-eye structures is lifted above the crests of the waves.

6.2. **Growing groups.** We next consider the case where groups of waves for which the initial profile as well as the lower boundary condition can evolve under the influence of the wind flow above the wave. For the growing groups, the computational mesh is regenerated every 50 time steps, where each time step consists of 500 iterations and is increased as the waves become steeper. All the variables are then interpolated/extrapolated onto the new mesh. The growth factor for each wave within the group is $e^{\mathsf{K}c_i t}$, where K can be taken to be k, k_1 or k_2 and

$$c_i = 8c_g a/\lambda.$$

This choice of the complex wave celerity is chosen such that it yields a similar magnitude as that used in our earlier contribution [12]. A more physical expression may be deduced from parameterization expression for the energy-transfer rate from wind to waves, see [14].
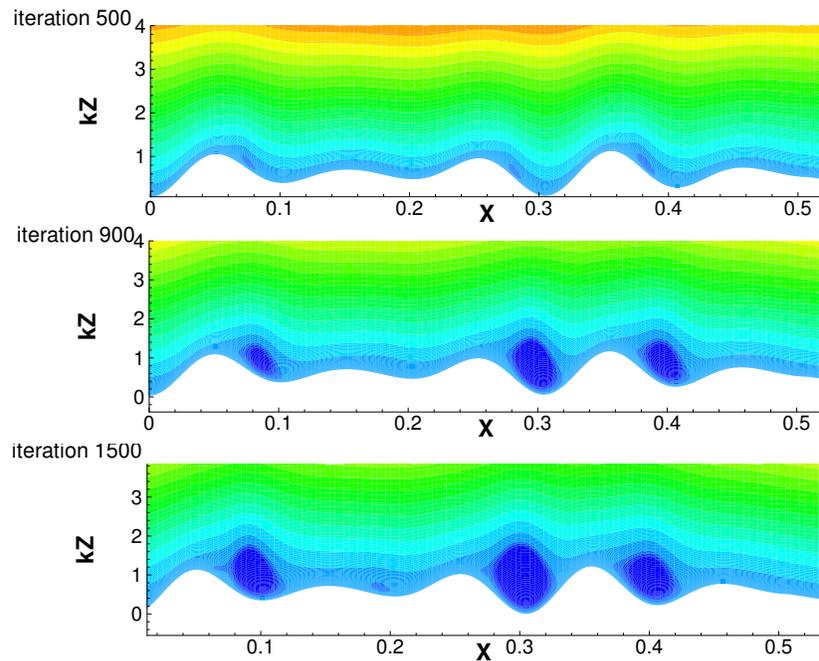
FIGURE 4. Contour plots of stream function over growing *group1* wave for a single value of the wave age $c_r/U_* = 5.75$. Steepest wave is depicted at the bottom.

In figure 4, we display the result of simulations for *group2* growing under the influence of the surrounding wind, for one fixed value of the wave age $c_r/U_* = 4.5$. As it can be seen, when the wave steepens, the cat's-eye structures are formed in the lee of the waves in the group. As the waves grow so do the cat's-eyes, and similar to our other computations for monochromatic waves and bimodal Stokes waves [11] (see also Sullivan *et al.* [4]), the critical height rises further up from the surface of the waves. It is also evident that the flow become more asymmetrical which shows how the air flow over the downwind part of the group is lower than over the upwind part.

7. **Conclusion**

The high-Reynolds-number stress model adopted in this study, successfully simulate the turbulent wind flow above growing and non growing groups of waves for different wave ages. Our simulations show that the height of the critical layer as well as the shape and positions of the cat's-eye structures that form in the lee of the waves of the groups are dependent on the wave age as it was previously shown for monochromatic and stokes waves with the same model [11]. As the waves of the groups are growing, so are the cat's-eye structures. The flow above the waves becomes asymmetrical. This asymmetry causes the critical layer height to be lower over the downwind part of the group what is in accordance with the conclusion of our earlier papers [12, 13]. The positive growth of the individual waves on the upwind part of the

wave group exceeds the negative growth on the downwind part. Hence, the effect of grouping on the critical layer produces a net horizontal force on the waves, in addition to the sheltering effect.

REFERENCES

[1] J.W. Miles, On the generation of surface waves by shear flows, *J. Fluid Mech.*, **3**, 185, 1957.

[2] M.J. Lighthill, Physical interpretation of the theory of wind generated waves, *J. Fluid Mech.* **14**, 385–398, 1962.

[3] F. Drullion, & S.G. Sajjadi, Interaction of wind with surface water waves, *Neural, Parallel, and Sci. Comp.* **22**, 303–314, 2014.

[4] P.P. Sullivan, J.C. McWilliams & C.H. Moeng, Simulation of turbulent flow over idealized water waves, *J. Fluid Mech.*, **404**, 47–85, 2000.

[5] S.G. Sajjadi, T.J. Craft, Y. Feng, A numerical study of turbulent flow over a two-dimensional hill, *Int. J. Numer. Meth. Fl.*, **35**, 1,2001.

[6] S. Fu, B.E. Launder and D.P. Tselepidakis, Accommodating the effects of high strain rates in modelling the pressure-strain correlation,*Rep. No. TFD/87/5*, Mechanical Engineering Department, UMIST, 1987.

[7] M.M. Gibson and B.E. Launder, Ground effects on pressure fluctuations in the atmospheric boundary layer, *J. Fluid Mech.*, **86**, 491, 1978.

[8] K. Hanjalic and B.E. Launder, A Reynolds stress model of turbulence and its application to thin shear flows, *J. Fluid Mech.*, **52**, 609, 1972.

[9] S.V. Patankar, *N*umerical Heat Transfer and Fluid Flow, Taylor & Francis, 1980.

[10] B.P. Leonard, A stable and accurate convective modelling procedure based on quadratic upstream interpolation, *Comp. Maths. Appl. Mech. Eng.*, **19**, 59, 1979.

[11] S.G. Sajjadi and F. Drullion, Numerical study of Turbulent flow over Growing Monochromatic and Stokes waves, *Advances and Applications in Fluid Mechanics*, **19**, 47, 2016.

[12] S.G. Sajjadi, J.C.R. Hunt, F. Drullion, Asymptotic Multi-Layer Analysis of Wind Over Unsteady Monochromatic Surface Waves, *Journal of Engineering Mathematics*, **84**, 73, 2014.

[13] S.G. Sajjadi, J.C.R. Hunt, F. Drullion, Growth of unsteady wave groups by shear flows, *Proc. of IMA Conference on Turbulence, Waves and Mixing, Kings College Cambridge, U.K., July 2016*, 79–84, 2016.

[14] S.G. Sajjadi, J.C.R. Hunt, F. Drullion. Turbulent shear flows over unsteady ideal and non-ideal water waves. To appear in *J. Fluid Mech.*, 2017.